Delgado, Ramón A.; Lau, Katrina; Middleton, Richard H. & Wigren, Torbjörn. "Networked delay control for 5G wireless machine-type communications using multiconnectivity" IEEE Transactions on System Control Technology, Vol. 27, Issue 4, p. 1510-1525 (2019).

Available from: http://dx.doi.org/10.1109/TCST.2018.2813328

Networked Delay Control for 5G Wireless Machine Type Communications Using Multi-Connectivity

Ramón A. Delgado , Katrina Lau, *Member, IEEE*, Richard H. Middleton, *Fellow, IEEE* and Torbjörn Wigren, *Senior Member, IEEE*

***Abstract*—Automatic control using ultra-reliable and low latency communication is one of the potential applications of the new fifth generation wireless systems. A remaining challenge is then to guarantee a low end-to-end delay with low jitter over combined internet and wireless interfaces that are packet switched and capacity optimized. The main novelty of the present paper is to introduce stringent delay control to meet this challenge, over simultaneous multiple data paths. The proposed multiple-input-multiple-output cascade control system is nonlinear since the dwell times of the transmission node queues used as actuators cannot be negative. Stability analysis based on integral quadratic constraint theory is therefore applied to characterize the global stability of the controller. The practical performance is evaluated with experiments using product like test bed C++ code. It is stressed that the proposed controller does not require inter-node time synchronization.**

***Index Terms*—5G mobile communication, URLLC, Delay, MIMO control, Networked Control, Nonlinear Systems, Stability.**

I. Introduction

FIFTH generation (5G) wireless systems aim to provide infrastructure for a number of new use cases, among these high performing wireless networked control [11], [28], [31], [32]. It is important to note that such ultra-reliable and low latency communication (URLLC) [2] functionality encompasses signals around the entire feedback control loop, not just conventional remote reference signal control over radio. Consequently, as noted in [34], the delay characteristics of the packet switched 5G end-to-end networks warrant renewed attention from the automatic control community. The novelty of the present work is believed to be the systematic application of feedback delay control to these 5G packet switched networks, simultaneously controlling the round trip delays over multiple data paths. The networked control applications operating over the 5G networks can then work under similar assumptions as when wired feedback control is applied, i.e. loop delays as low as the network allows with a minimal amount of jitter.

There are many commercial motivations for networked URLLC control, among these the possibility to reduce the need for cabling in manufacturing plants [19]. Apart from the associated cost reduction, removal of cabling is particularly beneficial in case of rotating machinery where slip-ring and rotary transformer based interfaces may otherwise be needed, see e.g. [4]-[7]. Other applications focus on situations where wireless connectivity provides unique possibilities, e.g. for remote surgery exploiting haptic feedback over a tactile internet [24], [29], [33].

The currently available techniques for delay control over the 5G wireless and wired internet include the transmission control protocol (TCP) and its augmentation with various kinds of active queue management (AQM) algorithms, see e.g. [36]. TCP aims for capacity optimization, while AQM is based on packet discards to mitigate problems with queue data volume overflow with less delay than TCP. A particular AQM algorithm for reduction of delay is random early detection (RED). RED starts to drop data packets randomly before the buffer threshold is exceeded. However, the analysis of [5] indicates that the jitter is increased instead, leaving the URLLC problem unsolved. Wireless factory automation and tactile internet feedback control applications over the new 5G networks thus require significantly lower round trip latencies and jitter levels than can be obtained with TCP and AQM, see [2], [19], [29], [46] and section II.B for a more detailed discussion. In addition, new impairments in typical 5G wireless URLLC architectures arise due to the combination of the non-guaranteed latency of packet switched networks, radio fading [13], and the need to use multi-point transmission to overcome radio shadowing in factory environments and at high carrier frequencies [11], [32], [44]. The problem with delay and jitter over the internet is a well studied subject, and there are techniques that go beyond TCP and AQM that could address some of the above impairments. One solution is to apply time-stamping of packets as a way to measure the delay, thereby allowing for delay control and for an increased robustness against jitter. An early approach can be found in [22]. That paper presents an observer based delay compensating networked controller. To handle varying delay, time synchronization between the controller node and the plant node is assumed. Such synchronization is a general prerequisite for the use of time-stamping of data to obtain delay robustness in networked control. A more recent approach to delay compensation can be found in [16]. There buffering is used to mitigate the effect of jitter in networked control applications. Work on multi-path architectures include e.g. [37]. That work discusses a statistical algorithm that trades off delay and time skew for *one way* downlink data like voice and

R. Delgado, K. Lau and R. H. Middleton are with the Priority Research Centre for Complex Dynamic Systems and Control, The University of Newcastle, Callaghan, NSW 2308, AUSTRALIA. e-mail: {ramon.delgado, k.lau, richard.middleton } @newcastle.edu.au .

T. Wigren is with L5GR Systems, Ericsson AB, Stockholm, SE-16480 Sweden. e-mail: torbjorn.wigren@ericsson.com.

Manuscript received December 15, 2016.

video. The URLLC feedback control applications are however concerned with *round-trip* delay, time skew and jitter, which is the case treated in the present paper.

One particular enhancement with respect to [37] is that the cascade controller of this paper enforces non-empty wireless transmission queues by constraining the inner loop queue dwell time reference values to be non-negative. This is important for URLLC feedback control applications since an empty transmission queue could stop the flow of control signals from the controller to the plant, thereby potentially corrupting e.g. a stabilizing control loop. This is not unusual in practice, where disturbances like radio fading can result in frequent very low queue dwell time reference values. This is very clearly illustrated by the numerical evaluation of section V, and by results reported e.g. in [40], [41], [42] and [45]. The non-negative constraint is particularly important when the time skew controller is adjusted to minimize the delay at the application layer, thereby operating with small transmission queue data volumes. The design of a linear controller that does not create negative queue dwell time reference values would require a back-off, resulting in operation with significantly larger wireless transmission queue data volumes. This is undesirable since it would increase the round trip delay experienced by the application.

The first contribution of the paper is therefore a new multiple-input-multiple-output (MIMO) networked round trip time (RTT) skew control algorithm. The round trip time skew controller exploits transmit data queues in the transmission nodes, in order to vary the dwell time of the application control signals in these queues. The controller exploits static decoupling, linear lead-lag design, and cascade control, to achieve a low computational complexity. An additional advantage is that the controller solves the data flow split problem at the controlling node, since the inner loop control signals are the downlink data rates that fully define the data flow split. In addition, no time synchronization between the involved nodes is required.

The round trip time skew controller is made non-linear by saturations that restrict the reference round trip time values of the inner loop controllers to be non-negative. A drawback with this is that the stability of the time skew controller becomes more complicated to assess. Fortunately, a stability analysis can still be carried out and the second contribution of the paper provides a MIMO stability analysis based on the theory of integral quadratic constraints (IQCs) [17], [23]. Conditions under which the closed loop time skew control system is globally stable are derived, and evaluated numerically. The evaluation indicates that the stability bounds are similar to those of [45] obtained with the classical Popov-criterion [39], and therefore IQC does not seem to produce overly conservative results. The numerical stability evaluation is performed for the controller tuning used in the experiments with the test bed C++ code. These experiments constitute the third contribution of the paper.

The problem at hand is a networked control problem, however the focus is on delay rather than on the quantization related problems of e.g. [3], [8], [14], [26]. In addition to the work of [5], [16], [22], [37] that was discussed above, work on delay with relevance for control over the wireless internet include e.g. [35], [40]-[43]. The reference [43] provides a stability analysis of the inner loop controllers that are controlled by the outer loop of the MIMO cascade controller of the present paper. The references [40]-[42] present alternative inner-loop control schemes. The paper [45] discusses a downlink time skew controller for dual connectivity in the 4G cellular long-term evolution (LTE) system. A linear analysis of disturbance rejection properties, related to the control system of [45], appears in [20], with a corresponding IQC stability analysis including nonlinearities presented in [10]. The works of [10], [20], [45] differ from the present paper in that other non-linear effects affect the control systems and that the inner loop controller of [40] is used. In addition, the stability analysis of [45] is based on the Nyquist- and Popov-criteria, [39], applied to a two path dual connectivity problem, rather than on the more general IQC theory of [17], [23] that is applied here. The time skew controller of [21] with a static reference value adjustment instead of a dynamic outer skew control loop could be modified to handle also the present control problem. In [25] the motivation for time skew control from a networked controller design perspective is discussed, based on a two path dual connectivity system architecture using URLLC. It also needs to be noted that the proposed controller is motivated by simplicity and computational complexity considerations. More advanced nonlinear controllers, e.g. based on model-predictive control [15], may therefore improve performance.

The notation uses boldface characters to indicate vectors and matrices. Whenever possible, dynamics is handled in the Laplace transform domain, using quantities that are functions of the Laplace variable . When handling nonlinear transformations a switch to the time domain is required which is stated directly in the paper. In addition, time domain signals are marked with an inverted caret as where indicates dependence of time.

The paper is organized as follows. Section II introduces the URLLC architecture. The proposed round trip time skew controller is discussed in Section III, followed by the stability analysis in Section IV. The control system is evaluated numerically in Section V. Conclusions end the discussion in Section VI.

II. 5G Wireless URLLC with Multi-node Connectivity

A. Networked URLLC Architecture

As discussed in the introduction, wireless 5G networks will be used for a variety of feedback control applications, often requiring an architecture that supports centralized closed loop controllers operating on cloud servers. The introduction of the model architecture of Fig. 1, where a controller node is connected to several plant nodes over multiple wireless interfaces served by multiple transmission nodes supports this requirement. The controller node is thus able to control one or more plants, connected to interface units denoted user equipments (UEs) in Fig. 1. The controller node is connected to the transmission nodes over network interfaces, implemented with e.g. optical fiber, copper wire or wireless backhaul [30].

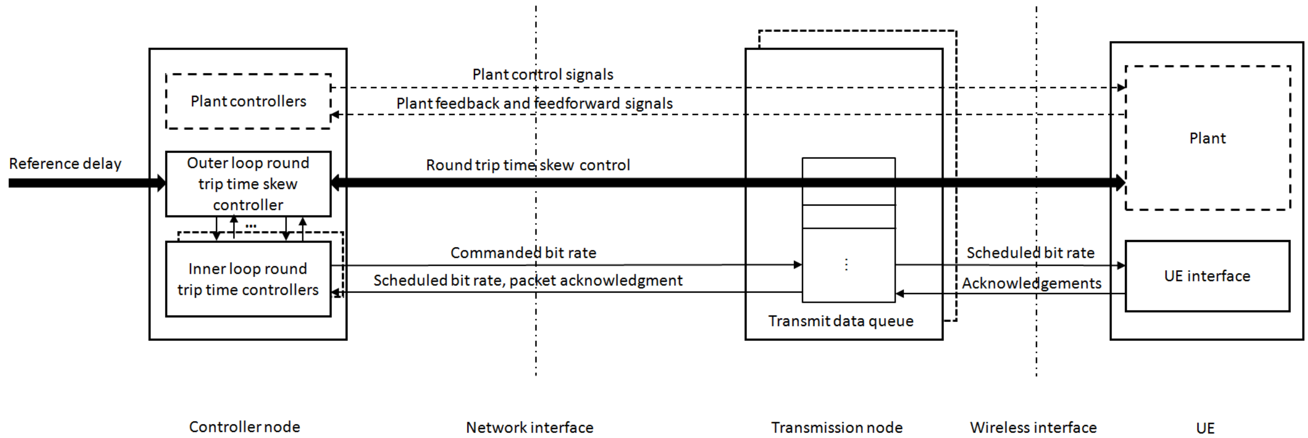

Fig. 1. The architecture of the URLLC round trip time skew control system. The remaining parts indicate the underlying round trip time skew control layer. A single plant node is shown in the figure, however the URLLC round trip time control architecture is designed to support several such nodes.

The transmission nodes each serve a wireless 5G interface connecting to the plant node interface which is essentially the radio interface of a 5G UE.

The URLLC application layer is marked with dashed boxes and lines, and it is at this layer where plant controller commands are sent from the plant controller to the plants and where feedback signals are sent back from the plants to the plant controller. The transmission of controller commands and feedback information is performed unaware of the lower data bearer layer details. Application controllers can therefore be developed and deployed independently of the round trip time skew controller functionality that is the subject here.

As stressed in the introduction the 5G wireless networks are built on packet switched technology, meaning that delay properties are much less guaranteed than in wired circuit switched data connections. The function of the round trip time skew controller discussed in the paper is therefore to ensure that the lower layer data bearers offer services with as low delay and jitter as possible to the application layer feedback control system. This means that the round trip time skew controller needs to measure the round trip delay over each transmission node and regulate the time differences to minimize the deviation from the time skew reference values. At the same time the round trip delay needs to remain close to the loop delay reference selected for the particular feedback control application. Disturbances working against this include varying network interface delays e.g. due to data traffic related load variations, and varying wireless data rates due to shadowing and fading over the 5G radio connections [13], [32], [36], [44]. In addition, the loop delay itself makes the control of the round trip time skew difficult.

The round trip time skew controller proposed in the paper uses the wireless transmit data queues of Fig. 1 as actuators to balance the round trip time of each data path of the connection between the controller node and the plant node. The round trip time skew control signals are the data rates by which data is sent over each network interface to the corresponding transmit data queue. In this way the dwell time of the data in each transmit data queue is varied in the way needed to balance the round trip time of each path. Note that the proposed controller applies cascade control, with one inner round trip time controller handling each path.

B. URLLC Requirements and Data Flow Control

There are multiple requirements on the URLLC architecture of Fig. 1. Among these are a low enough error probability and a sufficient capacity over the air interface, both of which are related to dimensioning. These aspects are not discussed further in this paper.

To motivate why control of delay and time skew as proposed in the present paper is of central importance for 5G URLLC, it is noted that a backbone of factory automation is currently provided by industry standard fieldbuses that exploit wired Ethernet connectivity [19]. The provided delay characteristics are of very high quality. The synchronization and delay characteristics of the isochronous data exchange modes of the corresponding networks define control- and feedback-signal exchange cycles as fast as a few hundred , with a jitter level, c.f. the PROFINET IO [46]. The motion controllers of industrial robots typically exploit such fieldbus services. Impairments that prevent the 5G URLLC systems from meeting at least parts of the state of the art wired performance must therefore be addressed for 5G URLLC to stay competitive. The impairments affecting the architecture of Fig. 1 include internet delay and jitter over the network interfaces. The transmit data queues needed to compensate for the fading and thereby rapidly varying radio channel capacity [13] contribute with packet queue dwell time induced delay and jitter. These impairments typically dominate over the wireless interface delays themselves [2]. In addition to this, multi-point transmission as shown in Fig. 1 is needed in factory environments to cover up for the very significant radio shadowing at 5G frequency bands [31], [32], [44]. The delay variations between different transmission paths then contribute further to the jitter level. To meet the latency of discussed for URLLC [2], over the architecture of Fig. 1, it is therefore concluded that time skew control is a highly relevant problem.

A further reason why jitter control is important in this context is that jitter at the data bearer layer translates to irregular sampling at the application control layer. This means, for example, that the exact relation between continuous time and discrete time obtained with zero-order-hold (ZoH) sampling [12] for linear systems is lost. The consequence is a need to use more computationally intense time varying control - or to add performance reducing error margins in the controller design [25]. It is finally noted that the above requirements are also relevant for application of 5G URLLC to the tactile internet. The tactile internet is expected to include a variety of wireless augmented reality and virtual reality functionality for factory automation, construction, advanced gaming and remote medical care [29]. A common requirement is then a round trip latency well below at the application layer.

The 5G URLLC architecture of Fig. 1 therefore needs delay skew and delay control to secure at least the following general requirements:

- The round trip delay, including the effect of jitter, should be kept below a specified maximum value at the application layer.
- The round trip time differences between transmission paths at the application layer, including jitter, should be controlled towards specified values.

For very stringent round trip delay requirements the solution may require that the controller node and the transmission node be co-located. In many cases the controller node and the transmission nodes will however be connected with a network interface as depicted in Fig. 1. In this situation, stringent time skew control solves a number of practical problems. First, since the network interfaces would typically be internet interfaces that also carry other types of packet data traffic for multiple users [36], the associated network interface delay may change with the load thereby affecting the above two objectives. Another problem is that the technology used for the network interfaces may differ between transmission nodes, leading to very different nominal associated delays [30], [36]. In such situations the deployment could become more complicated by the need to adjust network interface delays against each other. The paper therefore proposes the use of automatic round trip time skew control, using the transmit data queues to control the round trip latency and round trip time skew according to the above two requirements. The details of the MIMO round trip time skew controller are described in the following section.

III. Round Trip Time Skew Control

A. MIMO Cascade Control Architecture

A block diagram of the proposed MIMO round trip time skew controller appears in Fig. 2, which shows the general case with transmission nodes and data paths. One of these data paths is selected as the reference data path, marked with the subscript . As is evident from the block diagram, the use of MIMO cascade control is proposed. The outer MIMO round trip time skew controller thus controls reference round trip time values, which are applied to the inner loops that control the round trip time of their respective data path, using a single-input-single-output (SISO) inner loop controller discussed below. All parts of the MIMO round trip time skew controller are located in the controller node, while the SISO inner loops are divided between the controller node and the transmission nodes depicted in Fig. 1. The transmit data queues are the entities that are manipulated for control of the round trip time skews between the data paths.

Remark 1: Note that control of different dynamic properties of a plant may require different bandwidths, thereby tolerating different loop delays. One solution in such situations could be to guarantee different round trip times over different data paths. In such situations it is not sufficient with a single round trip time skew reference value, set to zero. Instead, non-zero time skews would be needed, which is allowed here. Note also that the reference values need not be constants. One particular extension would be to apply extremum control [1] for on-line minimization of the total delay budget. In such a case the corresponding reference signal would become time varying.

B. Outer Loop

To describe the outer loop the round trip time skew control errors are first computed as

(1)

Here is the round trip time skew reference and is the measured time skew of the th data path as compared to the reference path . This time skew is obtained from feedback information delivered to the controller node by the inner loops, as described below. Since there are degrees of freedom, one for each data path, an additional control loop addressing the sum of the round trip times of the data paths is needed. The corresponding error is obtained as

(2)

where is the reference signal for the sum of round trip times and where is the measured sum of the round trip times of the data paths. The quantity can be thought of as a delay budget, available for distribution between the data paths. Some of this delay is consumed by the network interface and wireless interface delays, but the remaining amount of delay is available for distribution between the transmit data queues, to meet the round trip time skew control objective. The following example explains the idea:

Example 1: Assume that the delays of the network interface, the wireless interface and the UE amounts to for transmission node 1 and for transmission node 2. By allowing a total round trip time delay budget of , by setting , and by setting , the round trip time skew controller may solve a feasible control problem by steering towards the unique transmit data queue delays of for node 1, and for node 2. It is easily seen that the controller will be able to adjust the delay distribution using positive transmit data queue delays as long as the sum of the other interface delays does not exceed , for any of the two data paths. If that no longer holds, the control problem becomes infeasible.

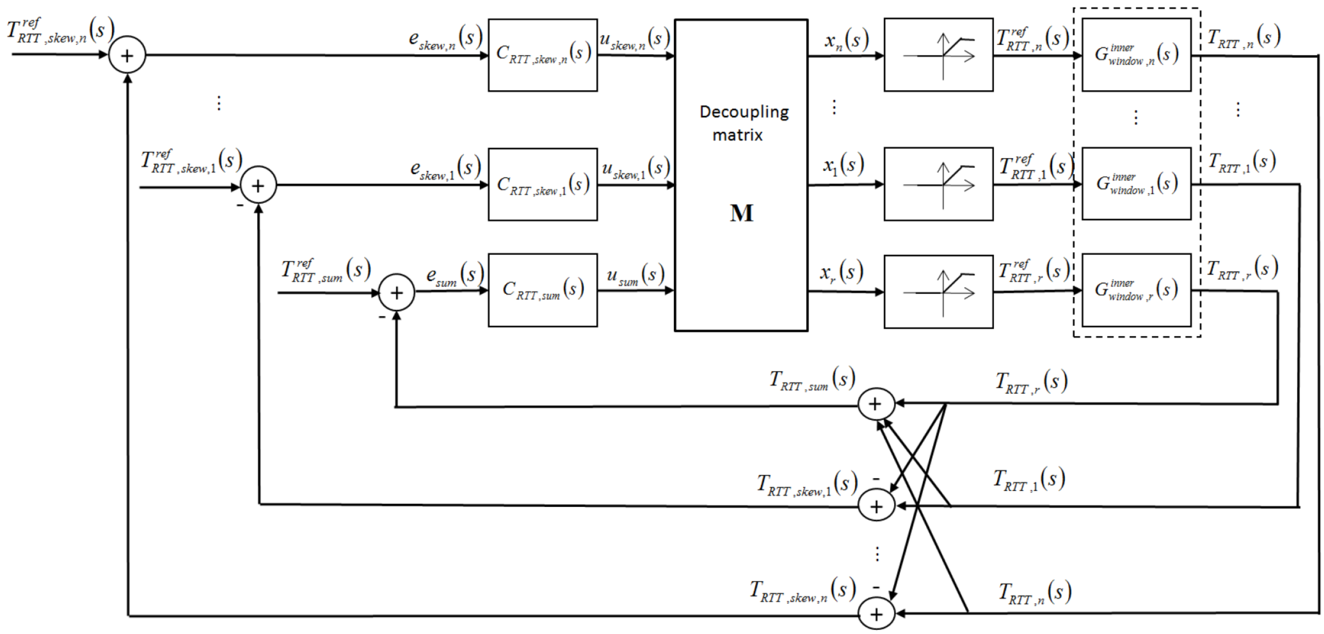

Fig. 2. The round trip time skew control loop, for an arbitrary number of transmission nodes. There is one inner loop controller for each transmission node.

The control errors are further processed by scalar feedback control filters to produce the control signals $u_{skew,i}(s)$, $i = 1, ..., n$, and $u_{sum}(s)$ that provide the input to the decoupling matrix block $\mathbf{M}$. The control signals are given by

$$u_{skew,i}(s) = C_{RTT,skew,i}(s)e_{skew,i}(s), \quad i = 1, ..., n, \tag{3}$$

$$u_{sum}(s) = C_{RTT,sum}(s)e_{sum}(s). \tag{4}$$

Here the design of the controller filters $C_{RTT,skew,i}(s)$, $i = 1, ..., n$, and $C_{RTT,sum}(s)$ is discussed in detail in section V. It can be noted that most scalar linear design techniques are immediately applicable, since the static decoupling matrix combines the control signals $u_{skew,i}(s)$, $i = 1, ..., n$ and $u_{sum}(s)$ by a linear mapping that decouples the data paths statically under assumptions discussed in the following subsection. The outputs from the decoupling matrix $\mathbf{M}$ consists of the following $n + 1$ signals

$$x_i(s) = \sum_{k=1}^{n} m_{i,k} u_{skew,k}(s) + m_{i,n+1} u_{sum}(s), \quad i = 1, ..., n, \tag{5}$$

$$x_r(s) = \sum_{k=1}^{n} m_{n+1,k} u_{skew,k}(s) + m_{n+1,n+1} u_{sum}(s), \tag{6}$$

where $m_{i,k}$ denotes a matrix element of $\mathbf{M}$. Since these signals are intended to provide the reference round trip times to the inner loop controllers, they are first constrained to be non-negative and bounded. Note that a switch to the time domain is needed to define the transformations that are given by

$$\begin{aligned}\check{T}^{ref}_{RTT,i}(t) &= \max(0.0, \min(\check{x}_i(t), T^{ref}_{max,i})) \\ &= sat_i(\check{x}_i(t)), \quad i = 1, ..., n,\end{aligned} \tag{7}$$

$$\check{T}^{ref}_{RTT,r}(t) = \max(0.0, \min(\check{x}_r(t), T^{ref}_{max,r})) = sat_r(\check{x}_r(t)). \tag{8}$$

Here $T^{ref}_{max,i}$, $i = 1, ..., n$ and $T^{ref}_{max,r}$ are the maximum reference values applied for the inner loops.

The reference signals of (7) and (8) provide the input to the $n+1$ inner loops. As seen from the outer loop these inner loops are modeled as linear filters $G^{inner}_{window,i}(s)$, $i = 1, ..., n$ and $G^{inner}_{window,r}(s)$, exploiting assumptions discussed in subsection III.D. Here it is sufficient to note that the inner loops provide the output round trip times

$$T_{RTT,i}(s) = G^{inner}_{window,i}(s) T^{ref}_{RTT,i}(s), \quad i = 1, ..., n, \tag{9}$$

$$T_{RTT,r}(s) = G^{inner}_{window,r}(s) T^{ref}_{RTT,r}(s). \tag{10}$$

The final step of the outer loop is the formation of the round trip time skew and sum feedback signals, given by

$$T_{RTT,skew,i}(s) = T_{RTT,i}(s) - T_{RTT,r}(s), \quad i = 1, ..., n, \tag{11}$$

$$T_{RTT,sum}(s) = \sum_{i=1}^{n} T_{RTT,i}(s) + T_{RTT,r}(s). \tag{12}$$

C. Static Decoupling

The use of $n + 1$ scalar linear controller filters builds on the assumption that the control of the data paths can be reasonably well decoupled. The approach here is to derive a static decoupling, applicable when the round trip time skew control loop is designed with a significantly lower bandwidth than the inner loops. In order to derive the static decoupling matrix $\mathbf{M}$ the following technical assumption is needed:

A1) The dwell time reference restriction to non-negative values is statically inactive.

It is stressed A1 is introduced *only* to motivate the static decoupling, the saturations of (7) and (8) are retained in all other parts of the paper. In particular, note that the simulations and the IQC stability analysis consider the combined effect of static decoupling and saturations without A1, as implied by the conditions of Theorem 2. The question of how well the static decoupling works in the dynamic case is addressed by simulations and by the IQC stability analysis in Section V.

Remark 2: It was noted in example 1 that needs to be large enough for the round trip time control problem to be feasible. In static cases A1 can then be expected to hold. In case is selected to be sufficiently large, the margin to negativity will be large enough for A1 to hold also in the dynamic case, as long as the closed loop system remains stable. However, selection of a value which is too large leads to a correspondingly larger loop delay which may be negative for the application controller performance. Therefore the tuning of is a compromise, which implies that the saturation may well be active in the dynamic case. This is a main motivation for the IQC stability analysis of the paper.

To derive , the following matrix relations are introduced, using A1, (5), (6), (9) and (10)-(12),

$$\vdots \qquad \vdots \tag{13}$$

$$\vdots \quad \ddots \quad \vdots \qquad \vdots \tag{14}$$

$$\vdots \quad \ddots \quad \vdots \qquad \vdots \tag{15}$$

Above and denote vectors or triangular matrix blocks with dimensions that are obvious from their location in the matrices they define. An insertion of (13) in (14), followed by an insertion of the result in (15) results in

$$\vdots \qquad \vdots \tag{16}$$

Next, the static situation is addressed under the assumption of perfect inner loops, i.e.

A2) , and .

The assumption A2 is motivated by the cascade structure of the round trip time skew control system.

It now follows from Fig. 2, A1, A2 and (16) that the round trip time and round trip time sum control loops become statically decoupled whenever

$$\tag{17}$$

where is the identity matrix of order . The matrix can be analytically inverted to give the result:

Theorem 1: Assume that A1 and A2 hold for the round trip time skew control system of Fig. 2. The control loops then become statically decoupled if

$$\vdots \quad \ddots \quad \ddots \quad \ddots \qquad \vdots \quad \vdots \quad \ddots \quad \ddots$$

D. Inner Loop

One instance of the inner round trip time control loop is depicted in Fig. 3. That control system is discussed in detail in [43] and the discussion here is limited to arrive at the assumptions leading to the transfer function model of the inner loops of Fig. 2. The reader is referred to [43] for further details. The transmission node indices are dropped in the discussion of the details of the inner loop.

As can be seen in Fig. 3, the inner loop controller is located in the controller node. It produces rate control commands that result in a transmission of data items with this rate, over the network interface to the transmission node, where the data ends up in the transmit data queue. The data item is then sent over the wireless interface to the UE. If it is correctly received a corresponding acknowledgement message is sent back from the UE over the wireless interface to the transmission node, from which it is sent back to the controller node to complete the inner loop data flow. Here the term 'data item' is used to allow a simultaneous discussion of the practical handling of data in terms of internet packets [36], and the modeling of the control loop dynamics where data items are to be interpreted as bits.

The inner loop control algorithm of Fig. 3 is a window based algorithm that controls the number of data items that are *in flight* as counted from the controller node to the UE, and

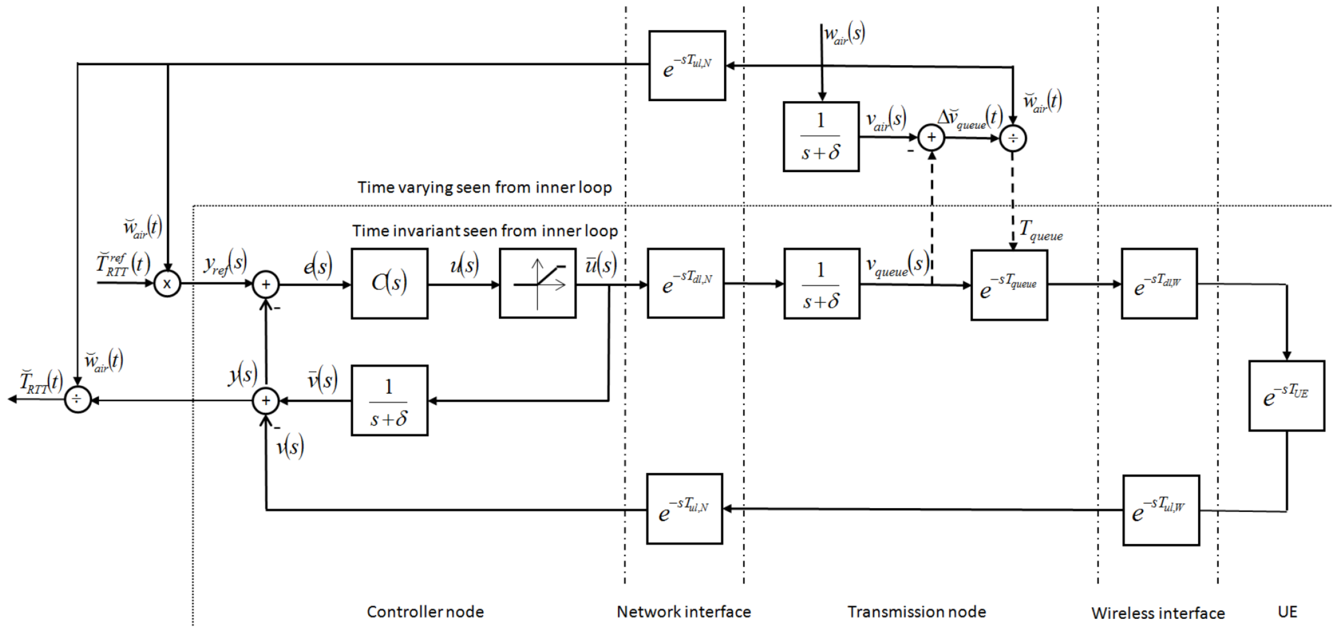

Fig. 3. The round trip time inner control loop, using data in flight feedback.

for the corresponding acknowledgement back, over a specific transmission node. To define the interface between the inner and outer loops the time and Laplace domains both need to be involved. The interface to the outer loop is accomplished by a multiplication of the dwell time reference value $\breve{T}_{RTT}^{ref}(t)$ by the scheduled wireless rate over the air interface, $\breve{w}_{air}(t)$, to obtain the reference value for the number of data items in flight as

$$y_{ref}(s) = \mathcal{L}\left(\breve{T}_{RTT}^{ref}(t)\breve{w}_{air}(t - T_{ul,N})\right), \tag{18}$$

where $\mathcal{L}(\cdot)$ denotes Laplace transformation and where $T_{ul,N}$ is the network interface delay from the transmission node to the controller node. At the output, the inverse transformation

$$\breve{T}_{RTT}(t) = \frac{\mathcal{L}^{-1}(y(s))}{\breve{w}_{air}(t - T_{ul,N})} \tag{19}$$

transforms the current number of data items in flight, $y(s)$, to the corresponding time, this being the round trip time.

The transformation (19) can of course also be obtained by keeping track of the transmission time of each data item sent in the downlink, the block diagram intends to illustrate the difference between the time invariant and time varying parts of the inner loop. It should be noted that the dynamics of the transmit data queue is not a part of the actual feedback loop of [43]. The reason is that the state variable defining the loop gain is rather the data item number. Therefore it is the delay of the transmit data queue that is a part of the control loop model. The queue generates this delay, thereby being an indirect part of the time varying part of the inner loop.

To describe the inner control loop in some detail the control error is formed as

$$e(s) = y_{ref}(s) - y(s). \tag{20}$$

The inner loop controller transfer function $C(s)$ then produces the data rate control signal

$$u(s) = C(s)e(s). \tag{21}$$

Since the data rate is non-negative (data items are not sent back) and limited by the capacity of the network interface channel [13], a saturation is used to generate the data rate by which data items are sent over the wireless interface. The saturation is given by

$$\breve{\bar{u}}(t) = \varphi(\breve{u}(t)) = \begin{cases} ku_{max}, & \breve{u}(t) \geq u_{max} \\ k\breve{u}(t), & u_{min} < \breve{u}(t) < u_{max} \\ ku_{min}, & \breve{u}(t) \leq u_{min} \end{cases} \tag{22}$$

where k is the gain, u_{min} is the lower saturation limit (typically 0.0) and u_{max} is the upper saturation limit. The signal $\bar{u}(s)$ is then integrated to provide the count of the data item number (here typically the number of the bit) that is currently sent over the network interface. This current data item (bit) number is denoted $\bar{\nu}(s)$ and it is obtained as

$$\bar{\nu}(s) = \frac{1}{s+\delta}\bar{u}(s). \tag{23}$$

The leakage factor $\delta > 0$ occurs since a so called active queue management algorithm (AQM) [36] may be overlaid, to improve end to end transmission control protocol (TCP) performance over the internet. AQM operates by intentionally discarding packets when the transmit data queue contents becomes too large, thereby introducing additional TCP feedback non-acknowledgement messages that reduce the round trip end-to-end latency, between the internet data source and the end user. The derivation of the leakage model that affects the controller node, the transmission node and the transmit data queue dynamics appears in [43] and is not repeated here. The incoming data item number of the transmit data queue,

$\nu_{queue}(s)$ is obtained from the data rate signal $\bar{u}(s)$, delayed over the network interface by $T_{dl,N}$, by leaky integration as

$$\nu_{queue}(s) = \frac{1}{s+\delta} e^{-sT_{dl,N}} \bar{u}(s). \quad (24)$$

The transmit data queue delay, T_{queue}, is modeled as a constant here, similarly to the other delays of the inner loop. This is motivated by the fact that the stability analysis of [43] requires such assumptions, and since the use of stable inner loop controllers is a main idea of the overall round trip time skew controller design. The required assumption is

A3) $T_{dl,N}$, T_{queue}, $T_{dl,W}$, T_{UE}, $T_{ul,W}$ and $T_{ul,N}$ are constant.

Here $T_{dl,W}$ is the downlink wireless delay, T_{UE} is the UE processing delay and $T_{ul,W}$ is the uplink wireless delay.

The validity of the assumption A3 for each separate delay needs further comments. The assumptions on the network interface delays $T_{dl,N}$ and $T_{ul,N}$ are reasonable, at least in cases without large loads and network interface congestion. The wireless interfaces $T_{dl,W}$ and $T_{ul,W}$ are designed to be small and in the sub-ms region in 5G, also in case of re-transmission [13]. They are therefore typically constant and never dominating. The same is true for the UE processing delay, T_{UE}. The exception is the transmit data queue delay, T_{queue}, which is dependent on the scheduled wireless rate and the commanded input data rate. In practice the queue delay will therefore not be constant. However, since i) the inner loop controller controls $\check{T}_{RTT}(t)$, ii) the other delays of the inner loop are typically close to constant, iii) the cascade control makes the variation of $\check{T}^{ref}_{RTT}(t)$ slow as compared to the inner loop dynamics, it can be argued that the inner loop controller itself tends to operate to keep T_{queue} constant. This argumentation shows that the model with constant delays, as stated by A3, is not an unreasonable one. The reader is referred to [43] for further details on the modeling of T_{queue}.

Following the loop back to the controller node now results in the equation

$$\nu(s) = \frac{1}{s+\delta} e^{-s(T_{dl,N}+T_{queue}+T_{dl,W}+T_{UE}+T_{ul,W}+T_{ul,N})} \bar{u}(s). \quad (25)$$

where $\nu(s)$ denotes the data item number (the bit number) of the latest acknowledged data item correctly received in the UE. The difference

$$y(s) = \bar{\nu}(s) - \nu(s) \quad (26)$$

is the feedback signal, representing the number of data items in flight. Insertion of (23) and (25) in this expression results in

$$y(s) = \frac{1}{s+\delta} \left(1 - e^{-s(T_{dl,N}+T_{queue}+T_{dl,W}+T_{UE}+T_{ul,W}+T_{ul,N})}\right) \bar{u}(s). \quad (27)$$

The linear loop gain of Fig. 3, from $\bar{u}(s)$ to $-u(s)$, then follows by a multiplication with the transfer function $C(s)$ of the inner loop controller to give

$$\hat{g}(s) = \frac{C(s)}{s+\delta} \left(1 - e^{-s(T_{dl,N}+T_{queue}+T_{dl,W}+T_{UE}+T_{ul,W}+T_{ul,N})}\right). \quad (28)$$

Together with the static nonlinearity of (22), this defines the inner closed loop dynamics. The structure of the loop and the infinite dimensional linear loop gain suggest that input-output stability theory is applicable to the inner control loop [39]. This stability analysis reveals the following major reason for the use of the nonlinear inner loop controller of Fig. 3,

Lemma 1 (Theorem 2 of [43]): Consider the control system defined by Fig. 3 in the case of proportional control. Assume that the conditions A1-A5 of [43] hold. Then, in case $\delta \rightarrow 0$, the control system obeys the Popov inequality, which implies that the control system of Fig. 3 is asymptotically (in δ) globally $\mathcal{L}_2$-stable for all delays $\{T_{dl,N}, T_{queue}, T_{dl,W}, T_{UE}, T_{ul,W}, T_{ul,N}\}$ and proportional controller gains $C > 0$.

Proof: See [43].

The inner loop controller thus has close to perfect stability properties, in case proportional control is applied.

In order to apply a straightforward linear design method to determine the time skew and time sum controller filters $C_{RTT,skew,i}(s)$, $i = 1, ..., n$, and $C_{RTT,sum}(s)$ of the outer loop, inner loop transfer functions need to be available. The inner loop controllers are however not linear. To allow such a linear design of the outer loop, the following approximation needs to be introduced:

A4) The saturation (22) can be replaced by $\mathcal{L}(k\check{u}(t))$ when $G^{inner}_{window,i}(s)$, $i = 1, ..., n$ and $G^{inner}_{window,r}(s)$ are computed.

An additional reason why the assumption A4 is made is that the IQC stability analysis of Section IV cannot handle arbitrarily cascaded nonlinearities. Therefore the stability analysis needs to be restricted to either a treatment of the saturations of the reference signals given by (7) and (8), or to a treatment of the inner loop nonlinearities of (22). The choice of the paper is expressed by A4. It can also be noted that the general assumption underpinning the cascade control paradigm is that the inner loop controllers can be treated as ideal as seen from the outer loop. The assumption A4 is thus in line with the cascade control paradigm, in the sense that the inner loops can be modeled with idealized models.

Using (27) together with A4 and Fig. 3 then immediately gives

$$G^{inner}_{window,i}(s) = \frac{k_i C_i(s)\left(1 - e^{-sT_{RTT,i}}\right)}{s + \delta_i + k_i C_i(s)\left(1 - e^{-sT_{RTT,i}}\right)}, \quad i = 1, ..., n, \quad (29)$$

$$G^{inner}_{window,r}(s) = \frac{k_r C_r(s)\left(1 - e^{-sT_{RTT,r}}\right)}{s + \delta_r + k_r C_r(s)\left(1 - e^{-sT_{RTT,r}}\right)}. \quad (30)$$

Here

$$T_{RTT,i} = T_{dl,N,i} + T_{queue,i} + T_{dl,W,i} + T_{UE,i} + T_{ul,W,i} + T_{ul,N,i}, \quad i = 1, ..., n, \quad (31)$$

$$T_{RTT,r} = T_{dl,N,r} + T_{queue,r} + T_{dl,W,r} + T_{UE,r} + T_{ul,W,r} + T_{ul,N,r}. \quad (32)$$

E. Nonlinear MIMO Round Trip Time Skew Control Model

A prerequisite for the IQC stability analysis of section IV is to transform the control loop of Fig. 2 into the standard representation that is used for IQC analysis. This is done for the case where the saturations of the inner loops are inactive. This is in line with the cascade control paradigm of the paper, allowing the inner loops to be idealized. It is stressed that it is not assumed that the decoupling operates as intended, that is a controller design assumption leading to the diagonal time skew controller filter (37). Note the dependence on both t and s need to be used below.

The relevant IQC theorems hold for the MIMO closed loop system

$$\begin{aligned} \mathbf{x}(s) &= \mathbf{G}(s)\mathbf{T}_{RTT}^{ref}(s) + \mathbf{e}(s) \\ \check{\mathbf{T}}_{RTT}^{ref}(t) &= \boldsymbol{\Delta}\check{\mathbf{x}}(t), \end{aligned} \quad (33)$$

cf. [17]. In (33) $\mathbf{G}(s)$ is a proper transfer function matrix with no poles in the right half plane, while $\mathbf{e}(s)$ is an external vector signal that is calculated below. The internal vector signals $\check{\mathbf{x}}(t)$ and $\check{\mathbf{T}}_{RTT}^{ref}(t)$ are also calculated below. Finally $\boldsymbol{\Delta}$ is a bounded and causal operator.

The vector signal $\mathbf{x}(s)$ is defined by

$$\mathbf{x}(s) = \begin{pmatrix} x_1(s) & \cdots & x_n(s) & x_r(s) \end{pmatrix}^T. \quad (34)$$

Similarly the internal signal $\mathbf{T}_{RTT}^{ref}(s)$ is defined by

$$\mathbf{T}_{RTT}^{ref}(s) = \begin{pmatrix} T_{RTT,1}^{ref}(s) & \cdots & T_{RTT,n}^{ref}(s) & T_{RTT,r}^{ref}(s) \end{pmatrix}^T. \quad (35)$$

With these definitions $\mathbf{G}(s)$ represents the linear matrix loop gain of Fig. 2, while the operator $\boldsymbol{\Delta}$ includes the effect of the saturation in the outer loop, built up from (7) and (8). Therefore, the bounded operator $\boldsymbol{\Delta}$ is given by

$$\boldsymbol{\Delta}\check{\mathbf{x}}(t) = \begin{pmatrix} sat_1(\check{x}_1(t)) & \mathbf{0} & 0 & 0 \\ \mathbf{0} & \ddots & \mathbf{0} & \mathbf{0} \\ 0 & \mathbf{0} & sat_n(\check{x}_n(t)) & 0 \\ 0 & \mathbf{0} & 0 & sat_r(\check{x}_r(t)) \end{pmatrix}. \quad (36)$$

The next step is to derive $\mathbf{G}(s)$. To do so, use is made of matrices $\mathbf{F}$ and $\mathbf{M}$ given by (15) and Theorem 1. Next, the application of decoupling and the separated design of the time skew/sum controller filter of each channel, leads to the following time skew controller filter matrix

$$\mathbf{C}_{skew}(s) = \begin{pmatrix} C_{RTT,skew,1}(s) & \mathbf{0} & 0 & 0 \\ \mathbf{0} & \ddots & \mathbf{0} & \mathbf{0} \\ 0 & \mathbf{0} & C_{RTT,skew,n}(s) & 0 \\ 0 & \mathbf{0} & 0 & C_{RTT,sum}(s) \end{pmatrix} \quad (37)$$

Following the MIMO loop counter-clockwise from $\mathbf{x}(s)$ to $\mathbf{T}_{RTT}^{ref}(s)$, using $\mathbf{C}_{skew}(s)$ and $\mathbf{G}_{window}^{inner}(s)$ given by (37) and (14), respectively, then gives

$$\mathbf{x}(s) = -\mathbf{M}\mathbf{C}_{skew}(s)\mathbf{F}\mathbf{G}_{window}^{inner}(s)\mathbf{T}_{RTT}^{ref}(s) + \mathbf{M}\mathbf{C}_{skew}(s)\mathbf{T}_{skew}^{ref}(s), \quad (38)$$

where

$$\mathbf{T}_{skew}^{ref}(s) = \begin{pmatrix} T_{RTT,skew,1}^{ref}(s) & \cdots & T_{RTT,skew,n}^{ref}(s) & T_{RTT,sum,r}^{ref}(s) \end{pmatrix}^T. \quad (39)$$

A comparison to (33) then gives the following linear MIMO loop gain and the external signal vector:

$$\begin{aligned} \mathbf{G}(s) &= -\mathbf{M}\mathbf{C}_{skew}(s)\mathbf{F}\mathbf{G}_{window}^{inner}(s), \quad (40) \\ \mathbf{e}(s) &= \mathbf{M}\mathbf{C}_{skew}(s)\mathbf{T}_{skew}^{ref}(s). \quad (41) \end{aligned}$$

All quantities needed for the IQC stability analysis are now defined.

IV. Stability Analysis using Integral Quadratic Constraints

Since the time skew control system contains delays it is infinite dimensional. A stringent treatment of the delays therefore rules out state space based Lyapunov methods for stability analysis of data flow delay control systems. Instead, input-output stability based methods, as pioneered in [47], [48], can be used, as in the SISO delay control cases of [40], [41], [42]. Loop transformations allow a treatment of some dual-input-dual-output time skew control cases as well, c.f. [25] and [45]. More recently, IQC analysis was used to analyse the general MIMO nonlinear time delay system of (33) [17]. The IQC method is therefore chosen for the stability analysis of the present paper.

The IQC stability analysis is performed in a number of steps. First the required definitions and the basic result of [17] are stated. Secondly, assumptions on the components of the skew control system of Fig. 2 and Fig. 3 are introduced. Finally, the basic result of [17] is used to formulate Theorem 2 below. Note that the MIMO model of section III.E is derived for arbitrary leakage coefficients $\delta_i \geq 0$, $i = 1, ..., n, r$. This general setting of the problem is also used in this section.

A. Tools of Analysis

The following definitions of [17], [23] are needed to set up the framework for the IQC analysis.

Definition 1: $\mathcal{L}_2^m$ denotes the space of $\mathcal{R}^m$-valued functions $\check{\mathbf{f}}(\cdot) : [0, \infty) \to \mathcal{R}^m$ of finite energy, i.e.

$$\|\check{\mathbf{f}}(\cdot)\|^2 = \int_0^\infty \check{\mathbf{f}}^T(t)\check{\mathbf{f}}(t)dt < \infty \quad (42)$$

Definition 2: The space $\mathcal{L}_{2e}^m$ is an extension of the space $\mathcal{L}_2^m$, whose members are $\mathcal{R}^m$-valued functions $\check{\mathbf{f}}(\cdot) : [0, \infty) \to \mathcal{R}^m$, such that their time truncation

$$\check{\mathbf{f}}_T(t) = \begin{cases} \check{\mathbf{f}}(t), & 0 \leq t \leq T \\ \mathbf{0}, & t > T \end{cases} \in \mathcal{L}_2^m \quad (43)$$

Definition 3: The feedback interconnection of $\mathbf{G}(s)$ and $\boldsymbol{\Delta}$ as in (33) is *well-posed* if it defines a causal map $\check{\mathbf{e}}(\cdot) \to (\check{\mathbf{v}}(\cdot), \check{\mathbf{w}}(\cdot))$ on $\mathcal{L}_{2e}^m$, i.e. for any $\check{\mathbf{e}}(\cdot) \in \mathcal{L}_{2e}^m$ there exists a solution $(\check{\mathbf{v}}(\cdot), \check{\mathbf{w}}(\cdot))$ that depends causally on $\check{\mathbf{e}}(\cdot)$. The interconnection is *stable* if, in addition, the inverse is bounded. This means that there exists a constant $C_{IQC} > 0$ such that

$$\int_0^T \left(\check{\mathbf{v}}^T(t)\check{\mathbf{v}}(t) + \check{\mathbf{w}}^T(t)\check{\mathbf{w}}(t)\right) dt \le C_{IQC} \int_0^T \check{\mathbf{e}}^T(t)\check{\mathbf{e}}(t)dt \tag{44}$$

In the rest of the paper the superscript m in $\mathcal{L}_{2e}^m$ is dropped.

A bounded operator $\mathbf{\Delta}$ is said to satisfy the IQC defined by $\mathbf{\Pi}(s)$, if for all $\mathbf{v}(s), \mathbf{w}(s)$

$$\int_{-\infty}^{\infty} \begin{bmatrix} \mathbf{v}(j\omega) \\ \mathbf{w}(j\omega) \end{bmatrix}^H \mathbf{\Pi}(j\omega) \begin{bmatrix} \mathbf{v}(j\omega) \\ \mathbf{w}(j\omega) \end{bmatrix} d\omega \ge 0 \tag{45}$$

with $\check{\mathbf{w}}(t) = \mathbf{\Delta}\check{\mathbf{v}}(t)$. The matrix $\mathbf{\Pi}(s)$ is denoted the multiplier defining the IQC.

Next assume that the following conditions hold:

C1) $\mathbf{G}(s)$ is a proper rational function with real coefficients without poles in the closed right half-plane.

C2) The interconnection of $\mathbf{G}(s)$ and $\tau\mathbf{\Delta}$ is well posed for all $\tau \in [0, 1]$.

C3) $\check{\mathbf{e}}(\cdot) \in \mathcal{L}_{2e}$.

C4) $\mathbf{\Delta}$ is a bounded causal operator.

C5) $\tau\mathbf{\Delta}$ satisfies the IQC defined by $\mathbf{\Pi}(s)$.

The main result in IQC theory is then:

Lemma 2: ([23]) Assume that C1-C5 hold. If there exists $\epsilon > 0$ such that $\forall\omega \in \mathcal{R} \cup \{\infty\}$

$$\begin{bmatrix} \mathbf{G}(j\omega) \\ I \end{bmatrix}^H \mathbf{\Pi}(j\omega) \begin{bmatrix} \mathbf{G}(j\omega) \\ I \end{bmatrix} \le -\epsilon I, \tag{46}$$

then, the feedback interconnection of $\mathbf{G}(s)$ and $\mathbf{\Delta}$ of (33) is stable.

To explain the conditions C1-C5, it is noted that C1 is a standard assumption in IQC theory which is straightforward to verify. A similar condition appears for the Popov and circle criteria when subject to saturating nonlinearities [39]. The condition C2 ensures that the interconnection *makes sense*. More specifically, it refers to the existence of unique solutions to the differential equations, and to the causality of such solutions. The condition C3 is standard in IQC theory. The conditions C4-C5 represent two well studied classes of bounded operators, see [17] and [23] for further details.

B. Assumptions on the Time Skew Controller

In the present paper, the numerical IQC analysis was carried out using rational approximations of all delays. The reason is that initial attempts to include the delays as parts of the operator $\mathbf{\Delta}$ produced conservative results. The applied approach instead increased the order of the rational approximations until the stability limits did not change significantly, thereby producing practically useful stability limits for moderate orders of the approximation, c.f. section V.C. Due to the suitability of the IQC model for the treatment of the saturations, there was then no need to switch to a Lyapunov based analysis [39] that could also have been applied in the finite dimensional numerical case. The following assumptions, additional to A1-A4, are therefore needed for the IQC analysis of the round trip time skew controller.

A5) The transfer functions $C_{RTT,sum}(s)$, $C_{RTT,skew,i}(s)$ are proper rational transfer functions without poles in the closed right half-plane.

A6) $\tilde{G}^{inner}_{window,i}(s)$, $i = 1, ..., n, r$ are proper rational transfer functions without poles in the closed right half-plane, where the time delays of $G^{inner}_{window,i}(s)$ have been replaced by a rational delay approximation of order $n_{delay,i}$ in $\tilde{G}^{inner}_{window,i}(s)$. The approximate transfer functions fulfil $\tilde{G}^{inner}_{window,i}(s) \rightarrow G^{inner}_{window,i}(s)$, $n_{delay,i} \rightarrow \infty$, $i = 1, ..., n, r$.

A7) $\check{\mathbf{T}}^{ref}_{skew}(\cdot) \in \mathcal{L}_{2e}$.

A8) The interconnection of $\mathbf{G}(s)$ and $\tau\mathbf{\Delta}$ is well posed for every $\tau \in [0, 1]$.

Assumptions A5 and A6 are needed to ensure that $\mathbf{G}(s)$ is consistent with C1. The assumption on the location of the poles of each controller, means that such controllers are required to be open loop stable. This bounded-input bounded-output stability condition can be easily addressed during the design of the controllers. Assumption A6 is introduced to idealize the inner control loops and to ensure that $\tilde{\mathbf{G}}^{inner}_{window}(s)$ is a rational transfer function. The intention with the use of rational delay approximations is to enable IQC stability analysis in a finite dimensional case, arbitrarily close to the infinite dimensional case when the delay approximation order tends to infinity. In the present paper Padé delay approximations [38] are used, exactly as in [41], [42]. A truncated inverted series expansion of e^{sT} could be used as well, where T is an arbitrary delay.

C. Verification of Integral Quadratic Constraint Conditions

In order to apply Lemma 2 it needs to be formally proved that the imposed conditions A3-A8 imply that C1-C5 hold. Clearly C1 follows from (40) if $\mathbf{C}_{skew}(s)$ and $\tilde{\mathbf{G}}^{inner}_{window}(s)$ are both proper without poles in the right half plane. This follows from A5 and A6 so C1 holds. Assumption A5 then ensures that $\mathbf{C}_{skew}$ is a bounded operator, therefore the assumptions A5 and A7 imply that the condition C3 is satisfied. The condition A8 then implies C2. The conditions C4 and C5 are known to be true from the analysis of [17], [23]. In addition to A5-A8, also A3-A4 needs to hold for the IQC analysis to be valid, a fact that is obvious from the previous treatment. Note that A1 and A2 are only used to support the derivation of the decoupling matrix. Since perfect decoupling is not assumed in the stability analysis, A1 and A2 are not needed in the following result:

Theorem 2: Consider the feedback interaction of (33) and assume that the conditions A3-A8 hold, where $n_{delay,i}$, $i = 1, ..., n, r$ are finite. Suppose that $\mathbf{\Delta}$ of (36) satisfy the IQC given by $\mathbf{\Pi}(s)$. Then, the feedback interconnection (33), with $G^{inner}_{window,i}(s)$, $i = 1, ..., n, r$, replaced by $\tilde{G}^{inner}_{window,i}(s)$, $i = 1, ..., n, r$, is stable if there exists $\epsilon > 0$ such that (46) holds $\forall\omega \in \mathcal{R} \cup \{\infty\}$.

Note that the condition (46) is an infinite-dimensional, frequency-dependent, linear matrix inequality. However, by using the Kalman-Yakubovich-Popov (KYP) lemma, the condition (46) can be converted to a finite-dimensional frequency-independent linear matrix inequality. The details are outlined in [23]. In addition, note that the MATLAB^{TM} toolbox IQC-beta [18] provides a convenient way to analyse the stability of systems using IQC.

Finally, the infinite dimensional delay limit is addressed by

Conjecture 1: Consider the feedback interaction of (33) and assume that the conditions A3-A8 hold, where $n_{delay,i} \rightarrow \infty$, $i = 1, ..., n, r$. Suppose that $\mathbf{\Delta}$ of (36) satisfy the IQC given by $\mathbf{\Pi}(s)$. Then, the feedback interconnection (33) is stable if there exists $\epsilon > 0$ such that (46) holds $\forall \omega \in \mathcal{R} \cup \{\infty\}$.

As indicated by the numerical results of section V.C, the stability limit of the infinite dimensional case appears to be reached for relatively low orders of the delay approximation. An order well below 10 seems to be sufficient in the treated example.

V. Numerical Results

The numerical results are based on C++ testbed code, that is intended to form the basis for product development. Since the 5G standards are still in development, it is not yet possible to obtain field results.

A. Test Code Implementation

The round trip time skew controller algorithm was implemented in C++, rather than in MATLAB. The advantage is that C++ code can be used for more tasks than MATLAB code. As for a MATLAB implementation, controller performance evaluation can be done off-line with C++ code. The same C++ code can then be integrated and run on product like hardware, using Ericsson's multi-core digital signal processing (DSP) architecture. This allows detailed profiling at DSP cycle level which is much more accurate than estimates obtained by counts of arithmetic operations. This fact is particularly important when computational complexity is evaluated for multi-core processors.

The testbed implements the inner loop window based controller used here and analysed in [43]. The lead-lag queue dwell time inner loop controller of [40] is also implemented. An arbitrary number of transmission nodes can be used, and it is possible to use any mix of the two implemented inner loop controllers. The tuning of the inner loop controllers can be parameterized either in terms of all the controller parameters, or in terms of a single parameter $T_{RTT}^{nominal}$ that represents the nominal round trip delay. All other controller parameters are then derived from the nominal round trip delay. This is very advantageous, since a single system parameter can then be used by the operator (i.e. the user) to set the controller parameters for nominal delays from hundreds of ms down to a fraction of a ms. To briefly explain how this is done, note that the tuning of a lead-lag controller starts by definition of the crossover angular frequency ω_c [40]. Noting that an increased delay typically requires a reduced angular crossover frequency, it follows that

$$\omega_c = \frac{C_{\omega_c}}{T_{RTT}^{nominal}}. \quad (47)$$

Here C_{ω_c} is a scale factor corresponding to a well working controller tuning. As it turns out, all lead-lag link parameters then follow from ω_c using the procedure of [40]. The round trip time skew and round trip time sum controller filters are selected to be lead-lag links, exactly as in [40]. Also these controller filters can be parameterized in terms of all controller parameters of the lead-lag link, or in terms of the nominal round trip delay.

The inner loop implementation embeds a simulation of each data transmission between the controller node and the transmission nodes. The delays in the downlinks and uplinks can be varied independently to simulate time variation, using buffers to implement transport delays. The inner loop implementation also simulates the transmit data queue of each transmission node, thereby connecting to the wireless interfaces and data rates that empty the transmit data queues. Any wireless simulator may be used for the generation of the wireless data rates, however the testbed code can also interface to external test files that provide the wireless data rate that affects each transmit data queue. Wireless interface delays and UE processing delays can also be introduced in the simulation. In this way the inner loop simulation provides the time evolution of $T_{dl,N}$, T_{queue}, $T_{dl,W}$, T_{UE}, $T_{ul,W}$ and $T_{ul,N}$. The inner loop simulation also keeps track of the data item number with separate delay buffers, a fact that allows the momentary value of $y(s)$ of (26) to be evaluated by the inner loop window controller of the paper. The inner loop controller simulation is capable of producing output data files readable by MATLAB. This allows a use of MATLAB for display of the obtained results, as described below. Input data rates to the controller node can be introduced with various traffic models, however this is beyond the scope of the present paper.

B. Detailed Time Skew Controller Design

To provide an illustration of the performance of the controller, a case with 3 transmission nodes is treated. The inner loop controllers are selected to be proportional controllers to allow application of Lemma 1. The proportional gains of the inner loops were chosen as $C_i = 1000.0$, $i = 1, ..., n$, $C_r = 1000.0$. That choice was evaluated with good results in [43]. Furthermore, $k_i = 1.0$, $i = 1, ..., n$, $k_r = 1.0$, $\delta_i = 0.0$, $i = 1, ..., n$, and $\delta_r = 0.0$ were chosen. In the design it is furthermore assumed that the nominal designing round trip delays for the inner loop controllers are $T_{RTT,i}^d = 10.0\ ms$, $i = 1, ..., n$, $T_{RTT,r}^d = 10.0\ ms$, where d indicates 'designing delay'. Using this information, the bode plot of $G_{window,1}^{inner}(s)$, $G_{window,2}^{inner}(s)$ and $G_{window,r}^{inner}(s)$ given by (29) and (30) can be computed. The Bode plot is depicted in Fig. 4. As can be seen the response is close to constant with a small phase loss up to almost $100\ Hz$, after which the gain and phase starts to oscillate. Obviously, this is an effect of the designing delay of $10.0\ ms$, reflecting the way the Nyquist plot circulates around the origin and passes the instability point $-1 + 0j$. Since the delay is not well known and may change in the present application, any robust outer loop round trip time skew controller design therefore needs to have a bandwidth low enough to attenuate the frequencies where the inner loop transfer functions vary rapidly.

Since decoupling is applied, each control channel is designed separately. This assumption means that the measure-

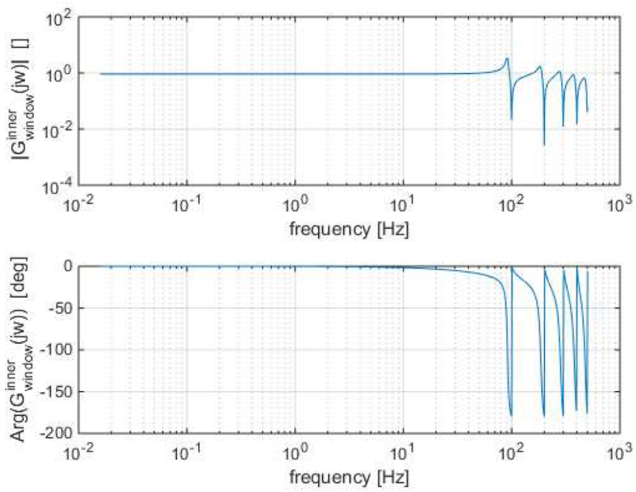

Fig. 4. Bode plot of the inner loop transfer functions. Note that the phase curve never passes -180 degrees. The reason is that the imaginary part of the frequency function is strictly negative for all ω, see [43].

ment combining and decoupling blocks $\mathbf{F}$ and $\mathbf{M}$ are neglected. This transforms the loop gain of (40) to the diagonal product $\mathbf{C}_{skew}(s)\mathbf{G}^{inner}_{window}(s)$. Since the three inner loops are assumed to be identical in the design, it follows that $C_{RTT,skew,1}(s) = C_{RTT,skew,2}(s) = C_{RTT,sum}(s)$. In the present work, the same lead-lag controller as in [40] is used, i.e

$$C_{RTT,skew,1}(s) = C_{RTT,skew,2}(s) = C_{RTT,sum}(s)$$
$$= K\frac{s+a}{s+\frac{a}{M}}N\frac{s+b}{s+bN}. \tag{48}$$

A complete algorithm for tuning of the controller parameters appears in [40]. The procedure is as follows. First the bandwidth and stability properties of the lead-lag controller is specified in terms of a desired crossover frequency for the loop gains of (28), and a desired phase margin at that crossover frequency. Here a crossover frequency of $f_c = 11.0\ Hz$ is specified, together with a phase margin of at least $90.0\ deg$. Next the time constant a and the amount of low frequency controller gain M of the lag-link is selected. Some experimentation revealed that $a = 0.25 \times \omega_c = 0.25 \times 2\pi f_c$ was suitable together with $M = 10$. Following this step the needed amount of phase advance is to be determined. However at the selected crossover frequency, the phase margin is well above the specification, and hence no phase advance is needed. The outer time skew controller filters are therefore simplified to

$$C_{RTT,skew,1}(s) = C_{RTT,skew,2}(s) = C_{RTT,sum}(s)$$
$$= K\frac{s+a}{s+\frac{a}{M}}, \tag{49}$$

i.e leaky integrating control. It then only remains to determine the gain factor K. This is done by applying (29) to solve for K using the crossover frequency condition

$$\left| K\frac{j\omega_c+a}{j\omega_c+\frac{a}{M}}G^{inner}_{window,i}(j\omega_c)\right| = 1, \tag{50}$$

TABLE I
STABILITY LIMITS IN TERMS OF T_{RTT} AS A FUNCTION OF C_i AND THE ORDER OF THE PADÉ APPROXIMATION.

	Order of Padé approximation					
C_i	3^{rd}	4^{th}	5^{th}	6^{th}	7^{th}	8^{th}
10^0	911 ms	866 ms	866 ms	866 ms	866 ms	866 ms
10^1	333 ms	300 ms	300 ms	299 ms	299 ms	299 ms
10^2	122 ms	100 ms	100 ms	100 ms	100 ms	100 ms
10^3	40 ms	33 ms	31 ms	31 ms	28.8 ms	29.4 ms
10^4	2 ms	1 ms	0.7 ms	0.7 ms	0.6 ms	0.56 ms

which results in the controller parameters $a = 17.28$, $M = 10.0$, and $K = 1.064$. Hence

$$C_{RTT,skew,1}(s) = C_{RTT,skew,2}(s) = C_{RTT,sum}(s)$$
$$= 1.064\frac{s+17.3}{s+1.73}. \tag{51}$$

The continuous time round trip time skew control system is finally discretized with Tustin's approximation [27]

$$s \longrightarrow \frac{2}{T_s}\frac{1-q^{-1}}{1+q^{-1}}, \tag{52}$$

where q^{-1} is the delay operator and $T_s = 1.0\ ms$ is the sampling period.

C. Stability

A numerical IQC stability analysis is performed in this subsection. The analysis quantifies how large round trip delays that can be tolerated before stability is compromized, assuming the controller design above. This serves to support the simulation results and to provide detailed engineering stability limits. Note that the stability conditions obtained by IQC analysis are not necessary, exactly as is the case when the Popov criterion is applied in [41], [42] and [45]. This means that the round trip time skew control system may still be stable, even if the IQC stability conditions are not met.

The IQC stability analysis was performed using the IQC-beta toolbox [18]. IQC stability tests were performed using $C_1 = C_2 = C_r = \{10^0, 10^1, \ldots, 10^4\}$. The delay approximations were selected to be Padé approximations of orders three to eight [38]. Table I shows the values of T_{RTT} for which stability of the round trip time skew control system is guaranteed. For this example, Padé approximations of fourth or higher order seems to provide reasonable stability limits. For the controller design used in the numerical simulation, i.e. $C_i = 1000$, $i = 1, ..., n, r$, stability of the round trip time skew control system can therefore be guaranteed when T_{RTT} is lower than $29\ ms$.

The computational cost associated with an IQC stability analysis is in general high [17], [18]. In the present application this is not a problem, since the stability analysis is typically done off-line during the setup of the time-skew controllers.

D. Test data generation model

Since there are not yet any complete 5G standard and products, simulated data needs to be used for evaluation of the proposed delay skew control algorithm. The third

TABLE II
DELAY PARAMETERS AT START OF SIMULATION

Parameter	Tx Node 0	Tx Node 1	Tx Node 2
$T^{ref}_{RTT,skew,i}$, $T^{ref}_{RTT,sum}$	40.0 ms	0.0 ms	0.0 ms
$T_{dl,N,i} + T_{dl,W,i}$	2.0 ms	10.0 ms	2.0 ms
$T_{ul,N,i} + T_{ul,W,i}$	1.0 ms	1.0 ms	1.0 ms
$T_{UE,i}$	1.0 ms	1.0 ms	1.0 ms

generation partnership project (3GPP) standardization has, however, evolved sufficiently far that it can be concluded that important parts resemble aspects of the 4G long term evolution (LTE) standard [9]. The radio access methods are e.g. similar, with orthogonal frequency division multiple access (OFDMA) being the choice in both cases. The consequence of this is that advanced system simulation tools of LTE may be tuned to resemble 5G multi-connectivity aspects.

Since the multi-connectivity flow control test code discussed in section V.A is stand alone, an interface between the re-tuned system simulator and the test code is needed. In this paper a single user full buffer scenario was assumed, meaning that the commanded bitrates will always be realizable by available physical data. In such a scenario, it is therefore the scheduled wireless rates over the multiple air-interfaces that drive the flow control test code. The interface is therefore provided by scheduled wireless rate signal files, generated by a properly re-tuned product system simulator.

To describe this data generation, the following brief description of the system simulator is given. The fading radio channel models for the air-interfaces were independent typical urban (TU) channel models with movement. The wireless rates are determined by the scheduler that runs fairly complicated algorithms that are beyond the scope of the present paper, see e.g. [9], [13] for an introduction. The scheduler is based on information of the channel qualities in the downlinks, that are measured by the mobile and obtained as feedback signals in terms of coarsely quantized channel quality indication (CQI) messages. The channel quality is affected by the received channel power spectral density in the mobile which in turn is affected by the fading and the path loss between the transmission nodes and the mobile. Other factors affecting the channel quality is the interference from neighbor cells and the capabilities of the mobile. The CQIs are input to the link adaptation on which the scheduled wireless rates are based. The link adaptation e.g. contains nonlinear tabulated mappings to arrive at quantities useful for the scheduling.

Wireless rate realizations were then generated by the above high fidelity system simulator. The user data was assumed to be transmitted over all three available transmission nodes simultaneously.

E. Performance

The reference transmission node was selected as number 0, with the two other transmission nodes being numbered as 1 and 2, respectively. The initial values of the delay parameters of the networked control system appear in Table II.

This means that the distributable delay budget is in total, since . In order to illustrate the performance and operation of the round trip time skew controller, the sum of the downlink interface delays of transmission nodes 1 and 2 were then varied as depicted in Fig. 5. The uplink interface delays and UE delays were constant. As can be seen from Fig. 5, the round trip time skew controller distributes the round trip times equally between the transmission paths, in line with the skew control reference values. It achieves this goal by adjusting the transmission node queue dwell times to compensate for the downlink interface delay variations, as is also evident from Fig. 5.

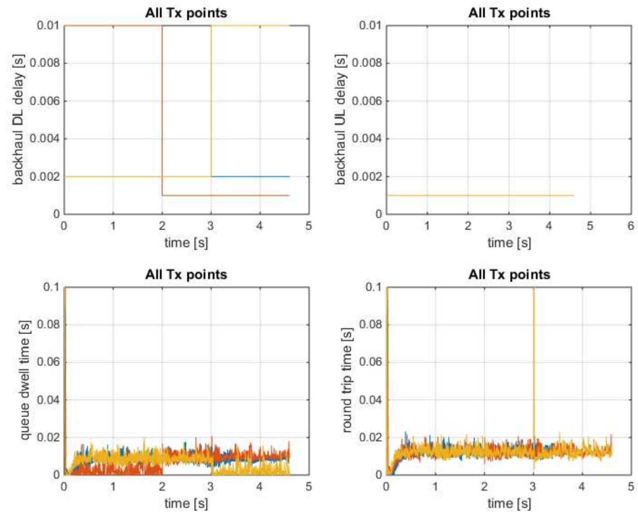

Fig. 5. The time evolution of the downlink interface delays (top left), the uplink interface delays (top right), the resulting queue dwell times (bottom left), and the resulting round trip times (bottom right). Transmission nodes 0, 1 and 2 are plotted blue, red and yellow, respectively. The spike at 3000 ms is believed to be a result of a transient in the delay generating queues of the simulator and not an effect of the controller.

To further analyse the way the algorithm operates, Fig. 6 - Fig. 8 provide detailed information about the inner loop operation of each transmission path. It can be seen that the queue dwell time of the reference node is kept constant, at about one third of the total delay budget. The inner loop controller achieves this goal by adjusting the queue data volume of the queue of transmission node 0. Transmission node 1 needs to use a small queue dwell time to compensate for the high downlink interface delay for the first 2 seconds of the simulation. It then quickly increases the queue dwell time when the downlink interface delay is reduced after 2 seconds. Again, this is done by adjustment of the queue data volume. Transmission node 2 on the other hand uses a high queue dwell time the first 3 seconds, while the queue dwell time is decreased after 3 seconds, to compensate for the increased downlink interface delay. It can be noted that the inner loop window controllers are very quick in performing the needed changes, which is believed to be a consequence of the use of high gain proportional control. Note that bit rate as well as queue data volume saturations occur, without any effect on stability which remains consistent during the simulation. The excellent practical stability properties are believed to be explained by the strong result of Lemma 1, together with a controller design reflecting Theorem 2.

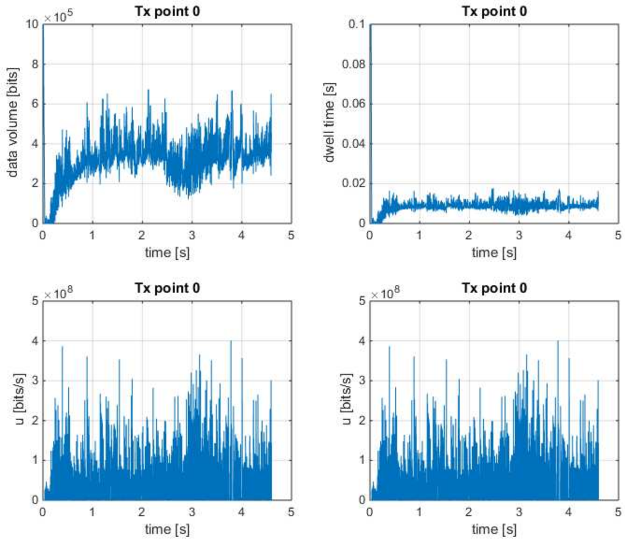

Fig. 6. The inner loop operation of transmission path 0, as a function of time.

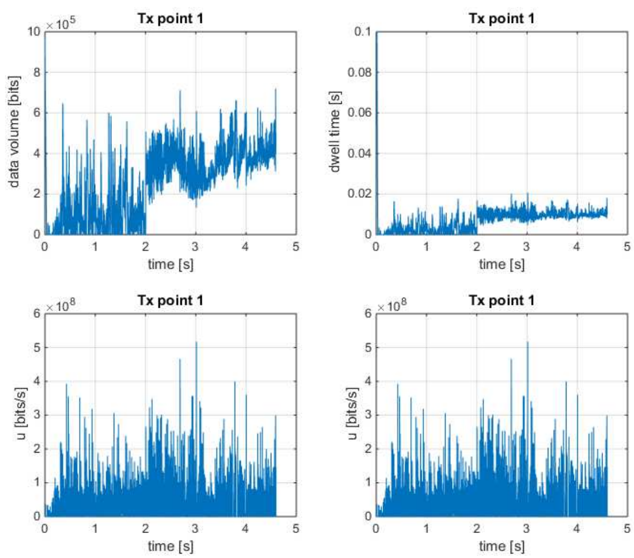

Fig. 7. The inner loop operation of transmission path 1, as a function of time.

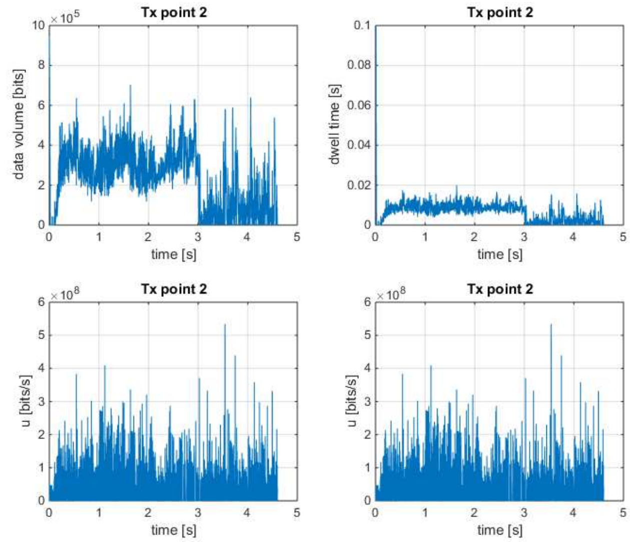

Fig. 8. The inner loop operation of transmission path 2, as a function of time.

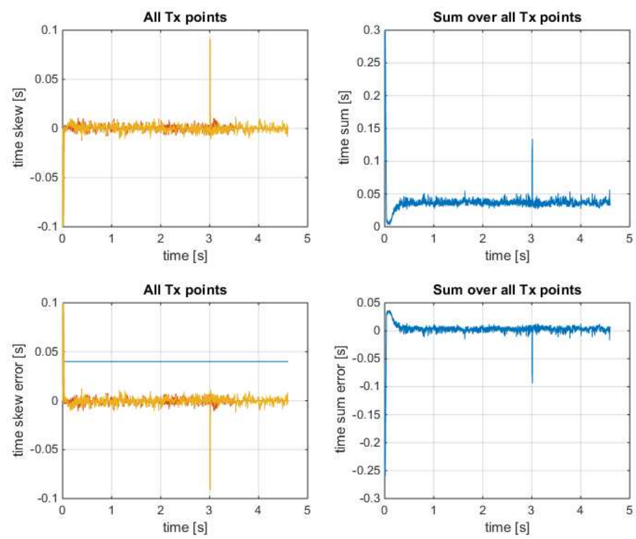

Fig. 9. The downlink interface delay variations, as a function of time. The spike at 3000 ms is believed to be a result of a transient in the delay generating queues of the simulator and not an effect of the controller.

As remarked in the introduction, the reference values for the transmission queue dwell times are constrained to non-negative values by the saturations in the loop. The need for this is evident from Fig. 7 and Fig. 8. Both figures clearly show that transient periods with zero queue data volume and zero queue dwell time do occur even with constraints. Without the constraints these periods would be of significantly longer durations.

The performance of the algorithm can be further studied in Fig. 9 that illustrates the time skew, the corresponding errors as well as the time sum and the corresponding error. It can be seen that the time skews are regulated towards as required. The remaining variations are due to the delays inherent in the control loops and the varying wireless rates. There is an initial transient of about before the round trip time skew controller has settled, after which the decoupling seems to work very well, also when the delays change. It can be noted that the length of the transient is consistent with the crossover frequency used in the design. Finally there is a spike at . This is believed to be due to the controller decreasing the dwell time of the queue of transmission node 2, at which time a significant saturation of the inner loop control signal takes place.

The standard deviations of the time skew control errors were and for transmission nodes 1 and 2, respectively. The time sum was controlled towards its setpoint of with a standard deviation of the error equal to . The initial transient and the spike were both removed when measuring the standard deviations.

As a final illustration of the operation of the round trip time skew controller, the various control signals are depicted in Fig. 10.

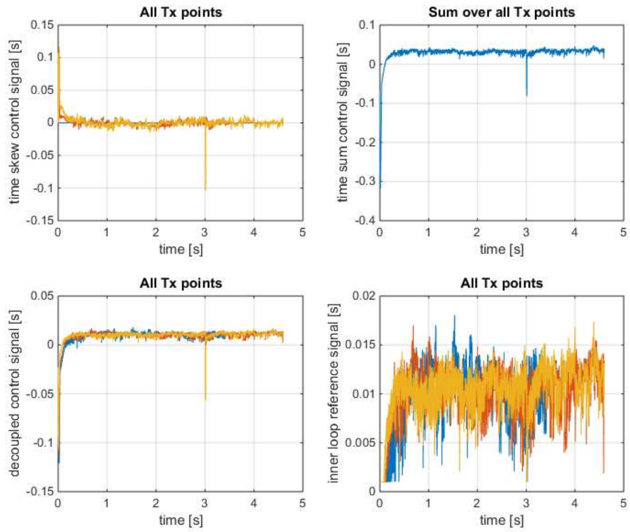

Fig. 10. The downlink interface delay variations, as a function of time. The spike at 3000 ms is believed to be a result of a transient in the delay generating queues of the simulator and not an effect of the controller.

F. Design guidelines

This paper, [10], [20] [25] and [45] treat two control objectives. The first objective aims at controlling the *one way* time skews from the controller node to the wireless interfaces. This is suitable for handling multi-point transmissions that terminate in the UE, like streaming video and augmented reality applications. Inter-node synchronization is required. As shown in [20] and [45], good disturbance decoupling and rejection require a symmetric network design and well designed inner loop controllers. The second control objective, treated here and in [25], aims at controlling the *round trip* time skews. This is suitable for handling URLLC feedback control applications in factory automation and over the tactile internet. A stability based design is recommended. An important aspect is that inter-node synchronization is not required.

VI. Conclusions

This paper has defined and discussed a new MIMO delay control problem that originates from the 5G wireless standards that are in development. The problem needs to be solved to enable high bandwidth networked feedback control over multiple wireless interfaces, supporting the use of URLLC for factory automation and the wireless tactile internet.

The main contribution of the paper is a new low complexity round trip time skew MIMO control algorithm. The controller exploits cascade control, where outer time skew controller filters provide round trip time references to the inner loops of each wireless transmission path, and where globally stable window based controllers serve as inner loop controllers. An important part of the contribution is that the round trip time skew controller also solves the nonlinear data flow split problem at the controller node, using mainly linear techniques. This follows since the inner loop control signals are the downlink network interface data rates that fully define the split. The second contribution of the paper is a stability analysis that exploits the integral quadratic constraint theory, to handle non-negativity constraints inherent in the MIMO controller. A further contribution reported on testbed experiments based on a three node scenario. The practical results of the testbed, with varying delays in the downlink interface chains, confirm the results of the stability analysis and show that the round trip time skew controller will be able to provide time skew control to within about 3 , using a sampling period of 1 . Note that inter-node time synchronization is not required.

There are many interesting research possibilities that may be explored, among these the use of more advanced controllers. One possibility is to replace the outer loop controller filters by more advanced linear controllers, e.g. based on robust control theory, or to apply non-linear model predictive control. Analysis of the theoretical performance bounds of the time skew control problem would also be interesting.

Acknowledgments

This research was supported under Australian Research Council's Linkage Projects funding scheme (project number LP150100757).

References

[1] K. B. Ariyur and M. Krstic, *Real-Time Optimization by Extremum-Seeking Control*. Hoboken, NJ: Wiley - Interscience, 2003.

[2] S. A. Ashraf, I. Aktas, E. Eriksson, K. W. Helmersson and J. Ansari, "Ultra-reliable and low-latency communication for wireless factory automation: From LTE to 5G", *IEEE 21st International Conference on Emerging Technologies and Factory Automation*, 2016.

[3] J. Baillieul, "Feedback designs for controlling device arrays with communication channel bandwidth constraints", *Proc. ARO Workshop Smart Structures*, Pennsylvania State Univ., PA, U.S.A., 1999.

[4] J. - M. Bockard and L. M. Reindl, "Ceramic and magnetic loop antennas for wireless interrogation of SAW resonators on rotation machinery", *Proc. IEEE Int. Workshop Antenna Technol.*, pp. 112-115, 2012.

[5] T. Bonald, M. May and J. - C. Bolot, "Analytic evaluation of RED performance" , *Proc. IEEE INFOCOM 2000*, vol. 3, pp. 1415-1424, 2000.

[6] T. L. Borim, J. Casey, T. Begalke and C. Ogawa, "Benefits of monitoring the rotor electrical quantities and transmitting by wireless communication", *Proc. IEEE Petroleum and Chemical Industry Committee Conf.*, pp. 1-11, 2015.

[7] R. F. M. Brandao, J. A. B. Carvalho and F. P. M. Barbosa, "Condition monitoring of the wind turbine generator slip ring", *Proc. 47th Int. Univ. Power Engineering Conf.*, pp. 1-6, 2012. DOI: 10.1109/UPEC.2012.6398673.

[8] R. W. Brocket and D. Liberzon, "Quantized feedback stabilization of linear systems", *IEEE Trans. Automat. Contr.*, vol. 45, no. 7, pp. 1279-1289, 2000.

[9] E. Dahlman, S. Parkvall, J. Sköld and P. Beming, *3G Evolution - HSPA and LTE for Mobile Broadband.* Oxford, UK: Academic Press, 2008.

[10] R. A. Delgado, T. Wigren, K. Lau and R. H. Middleton, "Stability properties of a MIMO data flow controller", *to appear in Proc. ACC 2018*, Milwaukee, USA, June 27-29, 2018.

[11] Ericsson AB, "5G Radio Access - Research and Vision", *Ericsson White Paper 284 23-3204*, June, 2013. Available: http://www.ericsson.com/res/docs/whitepapers/wp-5g.pdf.

[12] T. Glad and L. Ljung, *Control Theory.* Bodmin, UK: Taylor and Francis, 2000.

[13] A. Goldsmith, *Wireless Communications.* Cambridge, MA: Cambridge University Press, 2005.

[14] G. C. Goodwin, D. Quevedo and E. I. Silva "Architectures and coder design for networked control systems", *Automatica*, vol. 44, no. 1, pp. 248-257, 2008.

[15] G. C. Goodwin, M. M. Seron and J. A. DeDona, *Constrained Control and Estimation - An Optimization Approach*. London, UK: Springer-Verlag, 2005.

[16] R. Imai and R. Kubo, "Introducing jitter buffers in networked control systems with communication disturbance observer under time-varying communication delays", *IECON 2015*, pp. 2956-2961, 2015.

[17] C. - Y. Kao and A. Rantzer, "Stability analysis of systems with uncertain time-varying delays", *Automatica*, vol. 43, no. 6, pp. 959-979, 2007.
[18] C. - Y. Kao, A. Megretski, U. T. Jonsson and A. Rantzer, "A MATLAB toolbox for robustness analysis," *Proc. IEEE Int. Symposium on Computer Aided Control Systems Design*, Taipei, Taiwan, pp. 297-302, 2004.
[19] J. Kjellsson, A. E. Vallestad, R. Steigmann and D. Dzung, "Integration of a wireless I/O interface for PROFIBUS and PROFINET for factory automation", *IEEE Trans. Industrial Electronics*, vol. 56, no. 10, 2009.
[20] K. Lau, T. Wigren, R. Delgado and R. H. Middleton, "Disturbance rejection properties for a 5G networked data flow delay controller", *IEEE CDC 2017*, pp. 1681-1687, Melbourne, Australia, Dec. 12-16, 2017.
[21] K. Lau, T. Wigren, R. H. Middleton and R. Delgado, "Delay alignment for 5G multi connectivity", *submitted* , March, 2018.
[22] R. Luck and A. Ray, "An observer-based compensator for distributed delays", *Automatica*, vol. 26, no. 5, pp. 903-908, 1990.
[23] A. Megretski and A., Rantzer, "System analysis via integral quadratic constraints", *IEEE Trans. Automat. Contr.*, vol. 42, no. 6, pp. 819-830, 1997.
[24] T. Marugame, A. Kamikura, M. Ohnishi and M. Nakagawa, "Evaluation on effect of errors on haptic information in wireless communication systems", *Proc. Intelligent Robots and Systems*, vol. 3, pp. 2950-2955, 2003.
[25] R. H. Middleton, T. Wigren, K. Lau and R. Delgado, "Data flow delay equalization for feedback control applications using 5G wireless dual connectivity", *Proc. VTC 2017 Spring*, Sydney, Australia, June 4-7, 2017.
[26] G. N. Nair and R. J. Evans, "Stabilization with data-rate-limited feedback: tightest attainable bound", *Syst. Contr. Lett.*, vol. 41, no. 1, pp. 49-56, 2000.
[27] A. V. Oppenheim and R. W. Schafer, *Digital Signal Processing.* Englewood Cliffs, NJ: Prentice Hall, 1975.
[28] K. Pretz, "The future of communications networks", *the institute*, vol. 41, no. 1, pp. 6-7, 2017.
[29] K. Pretz, "Gerhard Fettweis: Developing 5G and beyond", *the institute*, vol. 41, no. 1, p. 14, 2017.
[30] Y. Qian, H. Asplund, J.-E. Berg and Z. Guo, "Non-line-of-sight 2.6 GHz relay backhaul channel performance: field test and analysis", *Proc. VTC 2012-Fall*, Quebec City, Quebec, Canada, 2012.
[31] T. S. Rappaport, "The renaissance of wireless communications in the massively broadband era", *Plenary talk, IEEE VTC 2012-Fall*, Quebec City, Quebec, Cananda, 2012.
[32] T. S. Rappaport, R. W. Heath Jr., R. C. Daniels and J. N. Murdock, *Millimeter Wave Wireless Communications*. Westford, Massachusetts: Prencice Hall, 2014.
[33] E. Ruffaldi, M. Satler, G. P. R. Papini and C. A. Avizzano, "A flexible framework for mobile based haptic rendering", *Proc. IEEE RO-MAN*, pp. 732-737, 2013.
[34] T. Samad, "Control systems and the internet of things," *IEEE Control Systems*, vol. 36, no. 1, pp. 13-16, 2016.
[35] Y. Song and J. Wang "Delay- and packet-disordering dependent H_∞ output tracking control for networked control systems", *Asian J. Contr.*, vol. 17, no. 3, pp. 917-931, 2015.
[36] R. Srikant and L. Ying, *Communication Networks - An Optimization, Control and Stochastic Networks Perspective*. Padstow Cornwall, UK: Cambridge Univeristy Press, 2014.
[37] C. J. Sreenan, J.-C. Chen, P. Agrawal and B. Narendran, "Delay reduction techniques for playout buffering", *IEEE Trans. Multimedia*, vol. 2, no. 2, pp. 88-100, 2000.
[38] M. Vajta, "Some remarks on Padé approximations", *Proc. third TEMPUS-INTCOM Symposium*, Veszprém, Hungary, 2000.
[39] M. Vidyasagar, *Nonlinear Systems Analysis*. Englewood Cliffs, NJ: Prentice-Hall, 1978.
[40] T. Wigren, "Robust $\mathcal{L}_2$ stable networked control of wireless packet queues over delayed internet connections", *IEEE Trans. Contr. Syst. Tech.*, vol. 24, no. 2, pp. 502-513, 2016. DOI: 10.1109/TCST.2015.2455933.
[41] T. Wigren, "Wireless feedback and feedforward data flow control subject to rate saturation and uncertain delay", *IET Control Theory & Applications*, vol. 10, no. 3, pp. 346-353, 2016. DOI: 10.1049/iet-cta.2015.0580.
[42] T. Wigren, "Low frequency sensitivity function constraints for nonlinear $\mathcal{L}_2$-stable networked control", *Asian J. Contr.*, vol. 18, no. 4, pp. 1200-1218, 2016. DOI: 10.1002/asjc.1241.
[43] T. Wigren and R. Karaki, "Globally stable wireless data flow control", *to appear in IEEE Trans Contr. Network Sys.*, 2018. DOI: 10.1109/TCNS.2016.2619906.
[44] T. Wigren, D. Colombi, B. Thors and J. - E. Berg, "Implication of RF EMF exposure limitation on 5G data rates above 6 GHz", *IEEE VTC 2015-Fall*, Boston, MA, 2015. DOI: 10.1109/VTCFall.2015.7390974.
[45] T. Wigren, K. Lau , R. Delgado and R. H. Middleton, "Delay skew packet flow control in wireless systems with dual connectivity", *to appear in IEEE Trans. Vehicular. Tech.*, 2018.
[46] Wikipedia, PROFINET, Nov. 2017. Available: https://en.wikipedia.org/wiki/PROFINET
[47] G. Zames, "Functional analysis applied to nonlinear feedback systems", *IEEE Trans. Circuit Theory*, vol. CT-10, no. 3, 1963.
[48] G. Zames, "On the input-output stability of time-varying nonlinear feedback systems, Part1: Conditions derived using concepts of loop-gain, conicity and positivity", *IEEE Trans. Automat. Contr.*, vol. AC-11, pp. 228-238, 1966.

Ramón A. Delgado received his professional title of Ingeniero Civil Electrónico and M.Sc. degree in Electronic Engineering from Universidad Técnica Federico Santa María, Chile, in 2009. He received the Ph.D. degree in Electrical Engineering from the University of Newcastle, Australia, in 2014. He is currently a research academic at the University of Newcastle. In his current role, Dr. Delgado is mainly focused on the current collaboration project between the University of Newcastle and the Swedish company Ericsson AB. His research interests include system identification, control, signal processing and optimisation.

Katrina Lau (M'07) received her B.E. (Elec) in 1997, B.Math in 1999 and Ph.D in 2003 from The University of Newcastle, Australia. Since then, she has been a research academic working on a number of industrial projects. She is currently working on next generation control and telecommunications problems with Ericsson AB. Her other research interests include fundamental performance limitations, switched control systems and stability analysis.

Richard H. Middleton (S'84-M'86-SM'94-F'99) completed his Ph.D. (1987) from the University of Newcastle, Australia. He was a Research Professor at the Hamilton Institute, The National University of Ireland, Maynooth from May 2007 till 2011 and is currently Professor at the University of Newcastle and Head of the School of Electrical Engineering and Computing. He has served as Program Chair (CDC 2006), co-general chair (CDC 2017), CSS Vice President Membership Activities, and Vice President Conference Activities. In 2011, he was President of the IEEE Control Systems Society. He is a Fellow of IEEE and of IFAC, and his research interests include a broad range of Control Systems Theory and Applications, including Communications Systems, control of distributed systems and Systems Biology.

Torbjörn Wigren (S'89-M'91-SM'98) received the M.Sc. degree (Engineering Physics) in 1985 and the Ph.D. degree (Automatic Control) in 1990, from Uppsala University, Uppsala, Sweden, where he is now adjunct Professor of Automatic Control. He is employed by Ericsson AB, Stockholm, Sweden, where he works with signal processing and control for 5G wireless systems. In 2007, he received the Ericsson Inventor of the Year award. His main research interests include nonlinear recursive identification and nonlinear control of networked systems.